Published in final edited form as:
Eur J Nucl Med Mol Imaging. 2012 January ; 39(1): 138–148. doi:10.1007/s00259-011-1930-x.

Positron emission tomography imaging of CD105 expression with ^{89}Zr-Df-TRC105

Hao Hong[1], **Gregory W. Severin**[2], **Yunan Yang**[1], **Jonathan W. Engle**[2], **Yin Zhang**[2], **Todd E. Barnhart**[2], **Glenn Liu**[3,4], **Bryan R. Leigh**[5], **Robert J. Nickles**[2], and **Weibo Cai**[1,2,4,*]

[1]Department of Radiology, University of Wisconsin - Madison, Madison, WI, USA

[2]Department of Medical Physics, University of Wisconsin - Madison, Madison, WI, USA

[3]Department of Medicine, University of Wisconsin - Madison, Madison, WI, USA

[4]University of Wisconsin Carbone Cancer Center, Madison, WI, USA

[5]TRACON Pharmaceuticals, Inc., San Diego, CA, USA

Abstract

Purpose—High tumor microvessel density (MVD) correlates with poor prognosis in multiple solid tumor types. The clinical gold standard for assessing MVD is CD105 immunohistochemistry on paraffin-embedded tumor specimens. The goal of this study was to develop an ^{89}Zr-based positron emission tomography (PET) tracer for non-invasive imaging of CD105 expression.

Methods—TRC105, a chimeric anti-CD105 monoclonal antibody, was conjugated to p-isothiocyanatobenzyl-desferrioxamine (Df-Bz-NCS) and labeled with ^{89}Zr. FACS analysis and microscopy studies were performed to compare the CD105 binding affinity of TRC105 and Df-TRC105. PET imaging, biodistribution, blocking, and ex vivo histology studies were performed on 4T1 murine breast tumor-bearing mice to evaluate the pharmacokinetics and tumor targeting efficacy of ^{89}Zr-Df-TRC105. Another chimeric antibody, cetuximab, was used as an isotype-matched control.

Results—FACS analysis of HUVECs revealed no difference in CD105 binding affinity between TRC105 and Df-TRC105, which was further validated by fluorescence microscopy. ^{89}Zr-labeling was achieved with high yield and specific activity. Serial PET imaging revealed that the 4T1 tumor uptake of ^{89}Zr-Df-TRC105 was 6.1 ± 1.2, 14.3 ± 1.2, 12.4 ± 1.5, 7.1 ± 0.9, and 5.2 ± 0.3 %ID/g at 5, 24, 48, 72, and 96 h post-injection respectively (n = 4), higher than all organs starting from 24 h post-injection, which provided excellent tumor contrast. Biodistribution data as measured by gamma counting were consistent with the PET findings. Blocking experiments, control studies with ^{89}Zr-Df-cetuximab, as well as ex vivo histology all confirmed the in vivo target specificity of ^{89}Zr-Df-TRC105.

Conclusion—Herein we report the first successful PET imaging of CD105 expression with ^{89}Zr as the radiolabel. Rapid, persistent, CD105-specific uptake of ^{89}Zr-Df-TRC105 in the 4T1 tumor was observed.

Requests for reprints: Weibo Cai, PhD, Departments of Radiology and Medical Physics, University of Wisconsin -Madison, Room 7137, 1111 Highland Ave, Madison, WI 53705-2275, USA wcai@uwhealth.org; Phone: 608-262-1749; Fax: 608- 265-0614.

Conflicts of interest BRL is an employee of TRACON Pharmaceuticals, Inc. The other authors declare that they have no conflict of interest.

Keywords

CD105/Endoglin; Positron emission tomography (PET); Tumor angiogenesis; ^{89}Zr; RadioimmunoPET; TRC105

Introduction

Positron emission tomography (PET) imaging with radiolabeled monoclonal antibodies (mAbs) has always been a dynamic area in molecular imaging [1, 2]. With decay half-life (3.3 d) well-matched to the circulation half-lives of antibodies (usually on the order of days), ^{89}Zr has been extensively studied over the last decade [2, 3]. The spontaneous gamma decay of ^{89}Zr, which gives rise to 909 keV photons, can be easily gated off by setting the energy window of a PET scanner. In addition, the E_{max} of 897 keV and E_{ave} of 397 keV for its positron emission can result in PET images with good spatial resolution. Recently, a feasibility study to determine the optimal dosage and timing of administering ^{89}Zr-labeled trastuzumab (a mAb recognizing the human epidermal growth factor receptor 2) in patients with metastatic breast cancer has been reported [4]. Excellent tumor uptake in metastatic liver, lung, bone, and even brain tumor lesions were observed.

Angiogenesis is a fundamental process in solid tumor development and metastasis [5]. Two of the most intensively studied angiogenesis-related targets are integrin $\alpha_v\beta_3$ and vascular endothelial growth factor receptors (VEGFRs), and several tracers targeting these two receptors are already in clinical investigation [6–8]. Another attractive target related to tumor angiogenesis is CD105 (endoglin), a 180 kDa disulphide-linked homodimeric transmembrane protein [9]. Various studies have suggested that CD105 is one of the most suitable markers for evaluating tumor angiogenesis [10, 11]. For example, high CD105 expression correlates with poor prognosis in more than 10 solid tumor types [9, 10]. These findings support the role of CD105 as an optimal marker of tumor angiogenesis, underscoring its clinical potential as a prognostic, diagnostic, and therapeutic vascular target in cancer.

Non-invasive imaging of CD105 expression represents a new paradigm for the assessment of anti-angiogenic therapeutics, as well as the investigation of the role of CD105 during tumor angiogenesis/metastasis [12, 13]. To date, literature reports on CD105 imaging are scarce, all are based on labeling anti-CD105 antibodies [13–22]. Another study investigated a ^{177}Lu-labeled anti-CD105 antibody for potential radioimmunotherapy applications [23]. We recently reported the first PET imaging of CD105 expression in a mouse breast cancer model with ^{64}Cu-labeled TRC105, a human/murine chimeric IgG1 mAb which binds to both human and murine CD105 [21]. When compared with other anti-CD105 antibodies, TRC105 has a very high avidity (with a K_D of 2 ng/mL) for human CD105 and is currently in a multicenter Phase 1 first-in-human dose-escalation trial in the United States [24]. Multiple Phase 2 therapy trials are planned or underway in patients with various solid tumor types.

The recent success of ^{89}Zr-labeled trastuzumab in metastatic breast cancer patients clearly suggested a promising future for ^{89}Zr-based PET tracers in the clinic [4]. To date, there is no PET tracer in clinical investigation for imaging CD105 expression. Therefore, the aim of this study is to investigate ^{89}Zr-labeled TRC105 in vitro and in vivo, with the ultimate goal of applying ^{89}Zr-labeled TRC105 for clinical PET imaging of tumor angiogenesis. ^{89}Zr-labeling of antibodies can be achieved through various types of chelators, primarily desferrioxamine B (Df) which can form a stable chelate with ^{89}Zr via the three hydroxamate groups [25, 26]. However, the multi-step procedure used in early studies of ^{89}Zr-labeled

mAbs is quite complicated and time-consuming, which makes it challenging to produce ^{89}Zr-labeled mAbs in compliance with current Good Manufacturing Practice (cGMP) for clinical investigations. Recently, a new bifunctional chelate was reported for ^{89}Zr labeling: *p*-isothiocyanatobenzyl-desferrioxamine B (Df-Bz-NCS) [27]. With this agent, labeling of ^{89}Zr has been significantly simplified from the initial 6-step strategy into a 2-step procedure, which was adopted for this study (Fig. 1).

Materials and methods

Reagents

TRC105 was provided by TRACON pharmaceuticals Inc. (San Diego, CA). Cetuximab (a human/murine chimeric IgG1 mAb that binds to human epidermal growth factor receptor [EGFR] but does not cross-react with murine EGFR [21]) was from Bristol-Meyers Squibb Company (Princeton, NJ). AlexaFluor488- and Cy3-labeled secondary antibodies were purchased from Jackson Immunoresearch Laboratories, Inc. (West Grove, CA). Df-Bz-NCS and Chelex 100 resin (50–100 mesh) were purchased from Macrocyclics, Inc. (Dallas, TX) and Sigma-Aldrich (St. Louis, MO), respectively. Water and all buffers were of Millipore grade and pre-treated with Chelex 100 resin to ensure that the aqueous solution was heavy metal-free. PD-10 desalting columns were acquired from GE Healthcare (Piscataway, NJ). All other reaction buffers and chemicals were from Thermo Fisher Scientific (Fair Lawn, NJ).

Cell lines and animal model

4T1 murine breast cancer, MCF-7 human breast cancer, and human umbilical vein endothelial cells (HUVECs) were purchased from the American Type Culture Collection (ATCC, Manassas, VA). 4T1 and MCF-7 cells were cultured in RPMI 1640 medium (Invitrogen, Carlsbad, CA) with 10% fetal bovine serum and incubated at 37 °C with 5% CO_2. HUVECs were cultured in M-200 medium (Invitrogen, Carlsbad, CA) with 1× low serum growth supplement (Cascade Biologics, Portland, OR) and incubated at 37 °C with 5% CO_2. Cells were used for in vitro and in vivo experiments when they reached ~75% confluence.

All animal studies were conducted under a protocol approved by the University of Wisconsin Institutional Animal Care and Use Committee. For the 4T1 tumor model, four- to five-week-old female Balb/c mice were purchased from Harlan (Indianapolis, IN) and tumors were established by subcutaneously injecting 2×10^6 cells, suspended in 100 μL of 1:1 mixture of RPMI 1640 and Matrigel (BD Biosciences, Franklin lakes, NJ), into the front flank of mice [28]. Tumor sizes were monitored every other day and mice were used for in vivo experiments when the diameter of tumors reached 5–8 mm (typically 1–2 weeks after inoculation).

Production of ^{89}Zr-oxalate

^{89}Zr-oxalate was produced according to the literature procedure with minor modifications [29]. Briefly, natural yttrium foil (250 μm, 99.9%) was irradiated with a proton beam to create ^{89}Zr via the ^{89}Y(p,n)^{89}Zr reaction, using a 11.4 MeV CTI RDS 112 cyclotron. Irradiations typically lasted for 2 h with a current of ~ 5 μA, yielding 280–320 MBq of ^{89}Zr on the yttrium target. The foil was then dissolved in concentrated HCl (ultrex grade, Mallinckrodt), diluted to < 2M HCl, and passed through 50–100 mg of hydroxamate resin. After washing the resin with 2M HCl and water, elution from the column was performed with 1M oxalic acid (trace metals grade, Sigma), where typically > 90% of the radioactivity was eluted in 1 mL. To calculate the specific activity of ^{89}Zr, the procedure above was performed on a non-irradiated yttrium foil, and the eluate was analyzed by inductively

coupled plasma mass spectroscopy (ICPMS) to determine the total mass of cold Zr. Titration studies of ^{89}Zr-oxalate with Df mesylate (Calbiochem), analyzed by radioTLC, were also performed to validate the ICPMS results.

Df conjugation and ^{89}Zr-labeling

Detailed procedures for Df conjugation to mAbs and subsequent ^{89}Zr-labeling have been reported previously [26, 27]. In brief, TRC105 or cetuximab was mixed with Df-Bz-NCS at pH 9.0 with a molar ratio of 1:3. The resulting Df-TRC105 and Df-cetuximab were purified with size exclusion chromatography. For radiolabeling, 74~148 MBq of ^{89}Zr-oxalate was neutralized with a 2 M Na_2CO_3 solution and added to a solution of Df-TRC105 or Df-cetuximab, where 0.05–0.35 mg of Df-mAb conjugate was used per 37 MBq of ^{89}Zr. The total reaction volume was adjusted to 2 mL with 0.5 M HEPES buffer (pH 7.1~7.3) and the reaction mixture (pH 6.8~7.2) was incubated for 1 h at room temperature (RT) with constant shaking. ^{89}Zr-Df-TRC105 and ^{89} Zr-Df-cetuximab were purified using PD-10 columns, where normal saline with 5 mg/mL of gentisic acid was used as the mobile phase. The radioactive fractions containing ^{89}Zr-Df-TRC105 or ^{89}Zr-Df-cetuximab were collected and passed through a 0.2 μm syringe filter for in vivo experiments.

Flow cytometry and microscopy studies

The immunoreactivities of TRC105, Df-TRC105, and Df-TRC105 after incubation in complete mouse serum at 37 °C, to HUVECs (high CD105 expression [17, 30]) and MCF-7 (CD105-negative [17]) cells were evaluated by fluorescence-activated cell sorting (FACS) analysis. Briefly, cells were harvested and suspended in cold PBS with 2% bovine serum albumin at a concentration of 5×10^6 cells/mL. The cells were incubated with TRC105 or Df-TRC105 (1, 5, or 15 μg/mL) for 30 min at RT, washed three times with cold PBS, and centrifuged at 1,000 rpm for 5 min. The cells were then incubated with AlexaFluor488-labeled goat anti-human IgG for 30 min at RT. Afterwards, the cells were washed and analyzed by FACS using a BD FACSCalibur 4-color analysis cytometer, which is equipped with 488nm and 633nm lasers (Becton-Dickinson, San Jose, CA) and FlowJo analysis software (Tree Star, Inc., Ashland, OR). HUVECs were also incubated with TRC105 or Df-TRC105 (2 μg/mL) and then examined under a Nikon Eclipse Ti microscope to validate the FACS results.

Imaging and biodistribution studies

PET scans were performed using an Inveon microPET/microCT rodent model scanner (Siemens Medical Solutions USA, Inc.). Each 4T1 tumor-bearing mouse was injected with 5–10 MBq of the PET tracer via tail vein and 5 minute static PET scans were performed at various time points post-injection (p.i.). The images were reconstructed using a maximum a posteriori (MAP) algorithm, with no attenuation or scatter correction. For each microPET scan, three-dimensional (3D) regions-of-interest (ROIs) were drawn over the tumor and major organs by using vendor software (Inveon Research Workshop [IRW]) on decay-corrected whole-body images. Assuming a tissue density of 1 g/mL, the ROIs were converted to MBq/g using a conversion factor (pre-determined using a 50 mL centrifuge tube filled with ~37 MBq of ^{89}Zr-oxalate as a phantom), and then divided by the total administered radioactivity to obtain an image ROI-derived percentage injected dose per gram of tissue (%ID/g). Another group of four 4T1 tumor-bearing mice was each injected with 2 mg of unlabeled TRC105 at 2 h earlier than ^{89}Zr-Df-TRC105 administration to evaluate the CD105 specificity of ^{89}Zr-Df-TRC105 in vivo (i.e. blocking experiment).

To anatomically localize the radioactivity signal observed in PET, a few animals were also subjected to microCT scans. Immediately after PET scanning, animalswere transported to the microCT gantry, positioned, and scanned at a voxel resolution of 210 μm (scanning time:

7 min). Fiducial markers were used for co-registration and images were reconstructed using the vendor software (Inveon Acquisition Workshop; Siemens). The microCT and microPET datasets were loaded into IRW and fiducial markers were co-registered for alignment of datasets.

Biodistribution studies were carried out to confirm that the quantitative tracer uptake values based on PET imaging truly represented the radioactivity distribution in tumor-bearing mice. After the last PET scans at 96 h p.i., mice were euthanized and blood, 4T1 tumor, and major organs/tissues were collected and wet-weighed. The radioactivity in the tissue was measured using a gamma-counter (Perkin Elmer) and presented as %ID/g (mean ± SD). In addition, another group of four mice were injected with ^{89}Zr-Df-TRC105 and euthanized at 24 h p.i. (when tumor uptake reached a peak) for biodistribution studies. The 4T1 tumor, liver, spleen, and kidney (i.e. tissues with significant uptake of ^{89}Zr-Df-TRC105) were also frozen for histological analysis.

Histology

Frozen tissue slices of 5 μm thickness were fixed with cold acetone for 10 min and dried in the air for 30 min. After rinsing with PBS and blocking with 10% donkey serum for 30 min at RT, the slices were incubated with TRC105 (2 μg/mL) for 1 h at 4 °C and visualized using AlexaFluor488-labeled goat anti-human IgG. The tissue slices were also stained for endothelial marker CD31 as described previously [31, 32]. After washing with PBS, the slices were incubated with rat anti-mouse CD31 antibody (2 μg/mL) for 1 h, followed by Cy3-labeled donkey anti-rat IgG for 30 min. All images were acquired with a Nikon Eclipse Ti microscope.

Statistical analysis

Quantitative data were expressed as mean ± SD. Means were compared using Student's t-test. P values < 0.05 were considered statistically significant.

Results

In vitro investigation of Df-TRC105

Df conjugation of TRC105 did not alter its CD105 binding affinity, as evidenced by both FACS analysis and fluorescence microscopy (Fig. 2). In FACS analysis of HUVECs (which express a high level of CD105), there were no observable differences between TRC105 and Df-TRC105 at 1 μg/mL or 5 μg/mL (Fig. 2a). The binding to HUVECs was specific, as neither TRC105 nor Df-TRC105 bound to CD105-negative MCF-7 cells, even at a much higher concentration of 15 μg/mL (Fig. 2a).

To evaluate its serum stability, Df-TRC105 was incubated in complete mouse serum at 37 C for up to a week. Based on FACS analysis using HUVEC cells, no degradation in CD105 binding affinity or specificity was observed even after 7 days of serum treatment (Fig. 2b), thus confirming the superb stability of Df-TRC105. Since ^{89}Zr-Df chelate is extremely stable (logK > 40), it is expected that ^{89}Zr-Df-TRC105 should maintain excellent stability in vivo. In addition to FACS analysis, fluorescence microscopy was also performed on HUVECs. No significant differences between TRC105 and Df-TRC105 were observed (Fig. 2c). Taken together, these in vitro studies confirmed that Df conjugation did not alter the antigen binding affinity or specificity of TRC105.

Specific activity measurement and ^{89}Zr-labeling

In each radiochemical separation > 200 MBq of ^{89}Zr was eluted from the hydroxamate resin in the first mL of oxalic acid. ICPMS analysis of the eluate indicated a cold mass of 1.02 μg

of Zr. Titration with Df mesylate gave consistent results, which showed a reactive equivalent mass of 1.10 μg of Zr in the same fraction. Therefore, the specific activity of ^{89}Zr produced for this study was 225.0 ± 23.7 MBq/μg of Zr (n = 6), which is comparable to the reported literature values for high specific activity ^{89}Zr (195–497 MBq/μg) [33]. The specific activity of ^{89}Zr can be further improved if longer irradiation time and/or higher beam power is used in future studies.

^{89}Zr-labeling including final purification using PD-10 columns took 100 ± 10 min (n = 10). The decay-corrected radiochemical yield was 62 ± 15 %, based on 0.05–0.35 mg of protein (Df-TRC105 or Df-cetuximab) per 37 MBq of ^{89}Zr, and the radiochemical purity was > 95%. The specific activity of both ^{89}Zr-Df-TRC105 and ^{89}Zr-Df-cetuximab was between 0.1 and 0.5 GBq/mg protein, assuming virtually complete recovery of the Df-mAb conjugates after size exclusion chromatography.

Small animal PET imaging

Due to the relatively long half-life of ^{89}Zr (3.3 d), which allowed for investigation of ^{89}Zr-Df-TRC105 over a significantly longer time period than ^{64}Cu-labeled TRC105 [21], the time points of 5, 24, 48, 72, and 96 h p.i. were chosen for serial PET scans after intravenous tracer injection,. The coronal slices that contain the 4T1 tumor are shown in Fig. 3a and representative PET/CT fused images of a mouse at 48 h p.i. of ^{89}Zr-Df-TRC105 are shown in Fig. 3b. The quantitative data obtained from ROI analysis are shown in Fig. 4. Due to the superb stability of the ^{89}Zr-Df conjugate, liver uptake of ^{89}Zr-Df-TRC105 was significantly lower at all time points examined than that observed for ^{64}Cu-DOTA-TRC105 (which may have certain degree of ^{64}Cu-transchelation, thereby increasing radioactivity accumulation in the liver) in our previous study in the same tumor model [21]. Meanwhile, blood pool activity was prominent at early time points (due to long circulation half-life of the antibody) which gradually declined over time. The liver uptake of ^{89}Zr-Df-TRC105 was 12.4 ± 2.1, 7.6 ± 1.5, 5.3 ± 0.2, 2.9 ± 0.1, and 2.3 ± 0.1 %ID/g at 5, 24, 48, 72, and 96 h p.i. respectively, while the radioactivity in the blood was 14.7 ± 2.5, 9.9 ± 1.9, 6.8 ± 0.7, 3.5 ± 0.5, and 2.0 ± 0.4 %ID/g at 5, 24, 48, 72, and 96 h p.i., respectively (n = 4, Fig. 4a). Tumor uptake of ^{89}Zr-Df-TRC105 was clearly visible as early as 5 h p.i. which reached a peak at around 24 h p.i. (6.1 ± 1.2, 14.3 ± 1.2, 12.4 ± 1.5, 7.1 ± 0.9, and 5.2 ± 0.3 %ID/g at 5, 24, 48, 72, and 96 h p.i. respectively; n = 4; Fig. 4a&d).

Administering a blocking dose of TRC105 two hours before ^{89}Zr-Df-TRC105 injection reduced the tumor uptake to background level ($P < 0.01$ at all time points examined when compared with mice injected with ^{89}Zr-Df-TRC105 alone; Fig. 3a, 4b&d), which clearly indicated CD105 specificity of the tracer in vivo. On the other hand, liver uptake of ^{89}Zr-Df-TRC105 was significantly higher at all time points examined when a blocking dose of TRC105 was injected (31.4 ± 7.3, 27.4 ± 3.8, 25.6 ± 4.4, 22.3 ± 7.1, and 8.9 ± 1.9 %ID/g at 5, 24, 48, 72, and 96 h p.i. respectively; n = 4). Radioactivity in the blood (2.2 ± 0.7, 1.3 ± 0.4, 0.9 ± 0.1, 1.1 ± 0.3, and 0.3 ± 0.1 %ID/g at 5, 24, 48, 72, and 96 h p.i. respectively; n = 4) was also much lower for the “blocking” group (Fig. 4b). Together, these data suggested much faster hepatic clearance of the tracer when most CD105 in the mice was already bound by pre-injected TRC105, thereby leaving no CD105 for ^{89}Zr-Df-TRC105 to bind to.

To further investigate the CD105 specificity of ^{89}Zr-Df-TRC105, ^{89}Zr-Df-cetuximab was used as an isotype-matched control. Both TRC105 and cetuximab are human/murine chimeric IgG1 mAbs. Since cetuximab does not cross-react with murine tissues, it serves as an excellent control for investigating tracer uptake in the tumor due to passive targeting only (i.e. the enhanced permeability and retention effect). As can be seen in Fig. 3a, 4c&d, the 4T1 tumor uptake of ^{89}Zr-Df-cetuximab is at the background level (< 3.5 %ID/g) and significantly lower than that of ^{89}Zr-Df-TRC105 at all time points examined ($P < 0.01$ at 5,

24, 48, and 72 h p.i.; $P < 0.05$ at 96 h p.i.; $n = 4$), which again confirms the CD105 specificity of ^{89}Zr-Df-TRC105 in vivo.

Biodistribution studies

A group of four mice were injected with ^{89}Zr-Df-TRC105 and euthanized at 24 h p.i. for biodistribution studies (Fig. 5a). Besides the liver, the kidneys also had significant tracer uptake at 24 h p.i., however the absolute uptake was significantly lower than that of the 4T1 tumor. Tracer uptake in all other tissues was also lower than the tumor. All other mice were euthanized after the last PET scans at 96 h p.i. for biodistribution and immunofluorescence staining studies to validate the in vivo PET data. Comparing the biodistribution data at 24 h and 96 h p.i., ^{89}Zr-Df-TRC105 uptake in most tissues declined significantly over time yet the tumor uptake remained prominent, which was indicative of specific interactions between an antibody and its antigen. Starting from 24 h p.i., 4T1 tumor uptake of the tracer was higher than that of all major organs in mice, thus providing excellent contrast with a tumor/muscle ratio of 24.8 ± 4.3 at 96 h p.i. ($n = 4$). Pre-injection of a blocking dose of TRC105 led to a significance decrease in 4T1 tumor uptake and increase in liver uptake of ^{89}Zr-Df-TRC105 ($P < 0.01$; $n = 4$; Fig. 5b), corroborating the PET findings.

A comparison of the biodistribution data between the two tracers at 96 h p.i. revealed that the uptake of ^{89}Zr-Df-cetuximab was higher than or similar to ^{89}Zr-Df-TRC105 in most organs except the 4T1 tumor (Fig. 5c), which again indicated specific tumor targeting of ^{89}Zr-Df-TRC105. Overall, the quantification results obtained from biodistribution studies and PET scans matched very well, confirming that quantitative ROI analysis of non-invasive PET scans truly reflected the tracer distribution in vivo.

Histology

Immunofluorescence CD105/CD31 co-staining of various tissues revealed that CD105 expression in the 4T1 tumor was primarily on the tumor vasculature, as evidenced by excellent co-localization of CD105 and CD31 staining and very weak signal on the 4T1 tumor cells (Fig. 6). Since CD105 is only expressed on actively proliferating endothelial cells, many of the mature vessels have significantly lower CD105 expression (indicated by arrowheads in Fig. 6) than in the neovasculature. Since the tumor vasculature is more actively proliferating in the peripheral region that in the center, tumor uptake of the tracer is rather heterogeneous (i.e. higher uptake in the peripheral region and lower uptake in the tumor center).

CD105 staining of mouse liver and spleen both gave very low signal, indicating that these tissues do not have significant level of CD105 expression. Thus, uptake of ^{89}Zr-Df-TRC105 in liver/spleen was largely unrelated to CD105 binding and more likely related to non-specific capture by the reticuloendothelial system and hepatic clearance of the tracer. Certain level of CD105 expression was observed in the kidney slices (mostly in the renal medulla) which likely caused appreciable renal uptake of ^{89}Zr-Df-TRC105, since full-length antibodies do not undergo renal clearance and the superb stability of ^{89}Zr-Df and Df-TRC105 will not give rise to significant amount of ^{89}Zr-containing low-molecular weight species. Taken together, the ex vivo findings corroborated the in vivo data of ^{89}Zr-Df-TRC105, warranting further investigation and application of this tracer.

Discussion

Over the last decade, mounting preclinical and clinical data have suggested the promising future of ^{89}Zr-based immunoPET in cancer patient management. The choice of Df as the chelator for ^{89}Zr is attractive because it has been safely used in the clinic for many years. In

the past and ongoing clinical studies, neither adverse reactions nor significant changes in blood and urine values were observed after injection of Df-containing conjugates [2, 3]. In addition, no antibody responses directed against the Df chelate were observed, indicating that its immunogenicity is very low [34]. With a new bifunctional chelator (i.e. Df-Bz-NCS) that recently became commercially available, it is expected that ^{89}Zr-based immunoPET will be the focus of more widespread future investigations.

The currently accepted standard method for quantifying angiogenesis is to assess MVD by performing CD105 immunohistochemistry on tumor tissue, an independent prognostic factor for survival in patients with many types of solid tumors [10, 11]. CD105 has the advantage of being selectively expressed on proliferating endothelial cells at significantly higher levels (up to 3×10^6 copies per cell) than other angiogenic targets such as the VEGFRs (less than 0.2×10^6 copies per cell) [30]. Non-invasive imaging of CD105 expression has the potential to accelerate anti-angiogenic drug development by providing a reliable measure of angiogenesis in the entire body as an intact system, thereby facilitating individualized treatment monitoring and dose optimization in animal models, clinical trials, and ultimately in the day-to-day management of cancer patients. Therefore, the goal of this study was to develop a CD105-specific PET tracer. We have achieved this goal and investigated TRC105 and its conjugates in vitro, in vivo, and ex vivo.

One key challenge in antibody labeling is to minimize the potential interference with its antigen binding affinity/specificity. There is only one lysine residue in each of the complementarity determining region (CDR) of TRC105 [11], which has a total of ~1400 amino acid residues and ~70 lysines, thus the possibility of Df conjugation at the lysine residue within the CDR is extremely low. Coupling of Df-Bz-NCS to mAbs was very efficient, and it has been reported that a reproducible chelate:mAb ratio of 1.5:1 could be obtained using only a three-fold molar excess of Df-Bz-NCS (which was adopted in this study) [27]. Such a low chelate:mAb ratio can adequately avoid alteration of the immunoreactivity (and pharmacokinetics) of TRC105, which is confirmed by FACS analysis and microscopy studies (Fig. 2).

The in vivo stability of radiometal-labeled antibodies is always a concern. To confirm that the tumor uptake of ^{89}Zr-Df-TRC105 visualized by non-invasive PET imaging was indeed CD105 specific, various control experiments (e.g. blocking study and the use of an isotype-matched control) and in vitro/ex vivo experiments (e.g. FACS, microscopy, and histological studies) were performed for validation purposes. Based on the available literature data, the ^{89}Zr-Df conjugate is very stable in vivo [2, 33]. Therefore, the key to in vivo stability and antigen binding affinity of an ^{89}Zr-based tracer lies in the stability of the Df-antibody conjugate (Df-TRC105 in this case). To investigate this aspect, we incubated Df-TRC105 in complete mouse serum at 37 °C for up to 7 days and observed no change in CD105 binding affinity/specificity based on FACS analysis, which confirmed the superb stability of the tracer.

The rationale for choosing the 4T1 murine breast cancer model in this study is that the parent antibody of TRC105 (SN6j, a mAb of murine origin which binds to CD105) has been shown to be an effective anti-angiogenic agent in this model [35]. Further, this is a rapidly growing tumor. Thus it has highly angiogenic tumor vasculature (Fig. 6) which is expected to provide sufficient target density for imaging applications. One limitation of this model is that the tumor vasculature is of murine origin. TRC105 has significantly higher affinity to human CD105 than its murine homolog [36]. Thus, the 4T1 tumor model is not optimal for testing TRC105. When compared with other antibody-based PET tracers [31, 37, 38], tumor uptake in this study is relatively low (~14 %ID/g at the peak). This is largely due to two facts. First, ^{89}Zr-Df-TRC105 targets the tumor vasculature but not the tumor cells. There are

significantly fewer tumor vascular endothelial cells than tumor cells, which are the targets of most antibodies used for cancer imaging. Second, TRC105's affinity to murine endothelial cells is lower than its affinity to human endothelial cells.

For future investigation, the following strategies may be adopted to better mimic the clinical situation and further improve the tumor uptake/contrast: stably transfect 4T1 cells with human CD105, use transgenic mice with human tumor vasculature, or test an anti-CD105 antibody that binds with high affinity to murine CD105. Follow-up studies are currently underway. In addition, studies have shown that tumor uptake of certain antibody-based PET tracers increased significantly when the specific activity of the tracer gets higher [39]. Therefore, with further improvement in the specific activity of ^{89}Zr and optimization of the radiochemistry, tumor uptake of ^{89}Zr-Df-TRC105 in the currently used 4T1 model may be further improved in future studies. Nonetheless, excellent tumor contrast was achieved in this study, which justifies optimism that this tracer may perform better in cancer patients than in the murine models reported here.

One interesting finding from this study was the clear difference between blood clearance and biodistribution patterns of the two PET tracers, where the uptake of ^{89}Zr-Df-cetuximabin the liver is much higher and faster than ^{89}Zr-Df-TRC105 (Fig. 3&4). Many factors can affect the circulation half-life of an antibody, and antigen binding is only one of them. The neonatal Fc receptor (FcRn), which binds to the CH_2-CH_3 hinge regions in the constant region (Fc) of IgG antibodies, plays a major role in their serum half-lives [40]. Although TRC105 and cetuximab are isotype-matched chimeric antibodies, their amino acid sequences in the Fc region may be different [41]. In addition, variable glycosylation patterns in the Fc regions also add to variability, in addition to variability in amino acid sequences. Thus, the immunocompetent Balb/c may recognize them with very different efficiency, which leads to different blood clearance rate and liver uptake.

In several other studies with ^{89}Zr-labeled antibodies, the tumor uptake reached a peak at around 24 h and remained stable for up to a week [33, 39]. Due to the fast growing nature of the 4T1 tumor used in this study, although the total tumor uptake of ^{89}Zr-Df-TRC105 is quite steady over a period of 4 days, the %ID/g values did drop over time since the tumor volume at 72 h and 96 h was 189 ± 34 % and 221 ± 25 % of its original volume at tracer injection (n = 4). It has been reported that $^{89}ZrCl_4$ is mostly taken up by the liver and ^{89}Zr-Df undergoes renal excretion [33]. The low liver and kidney uptake of radioactivity observed in this study further confirms the superb stability of ^{89}Zr-Df-TRC105 in vivo. Regarding potential clinical translation, quantitative correlation of PET tracer uptake with CD105 expression level would be highly desirable for treatment monitoring applications, as it would be ideal to non-invasively measure the changes of CD105 expression quantitatively, rather than qualitatively, in each individual patient upon anti-angiogenic therapies.

Conclusion

We have successfully investigated ^{89}Zr-labeled TRC105, a human-murine chimeric mAb recognizing both human and murine CD105, both in vitro and in vivo. Small animal PET imaging revealed rapid, persistent, CD105-specific uptake of ^{89}Zr-Df-TRC105 in the 4T1 tumor which was further validated by in vitro and ex vivo experiments. Since TRC105 is already in clinical investigation and therapeutic efficacy has been shown in various animal tumor models and certain cancer patients, this study identifies a new avenue for tumor angiogenesis-related research and warrants future clinical translation of ^{89}Zr-Df-TRC105, where it may be used to evaluate the pharmacokinetics, tumor targeting efficacy, dose optimization, and dose interval of TRC105 and TRC105-based cancer therapeutics in the

clinic. In addition, ^{89}Zr-Df-TRC105 may also be useful in patient selection and monitoring the therapeutic response for various anti-angiogenic therapies.

Acknowledgments

This work is supported, in part, by the University of Wisconsin Carbone Cancer Center, the NIH through the UW Radiological Sciences Training Program 5 T32 CA009206-32, NCRR 1UL1RR025011, a DOD BCRP Postdoctoral Fellowship, and a DOD PCRP IDEA Award. The authors also thank Dr. Jason P. Holland and Dr. Jason S. Lewis for sharing their expertise on ^{89}Zr production and radiochemistry, Dr. Anna Wu and Dr. David M. Goldenberg for helpful discussions, Dr. Martin Shafer at the University of Wisconsin State Hygiene Lab for performing the ICPMS study, and Dr. Jamey P. Weichert and Mohammed Farhoud for their help with the PET scans.

References

1. Wu AM. Antibodies and antimatter: the resurgence of immuno-PET. J Nucl Med. 2009; 50:2–5. [PubMed: 19091888]
2. van Dongen GA, Vosjan MJ. Immuno-positron emission tomography: shedding light on clinical antibody therapy. Cancer Biother Radiopharm. 2010; 25:375–85. [PubMed: 20707716]
3. Zhang Y, Hong H, Cai W. PET Tracers Based on Zirconium-89. Curr Radiopharm. 2011 in press.
4. Dijkers EC, Oude Munnink TH, Kosterink JG, Brouwers AH, Jager PL, de Jong JR, et al. Biodistribution of ^{89}Zr-trastuzumab and PET imaging of HER2-positive lesions in patients with metastatic breast cancer. Clin Pharmacol Ther. 2010; 87:586–92. [PubMed: 20357763]
5. Cai W, Chen X. Multimodality molecular imaging of tumor angiogenesis. J Nucl Med. 2008; 49 (Suppl 2):113S–28S. [PubMed: 18523069]
6. Cai W, Chen X. Multimodality imaging of vascular endothelial growth factor and vascular endothelial growth factor receptor expression. Front Biosci. 2007; 12:4267–79. [PubMed: 17485373]
7. Cai W, Niu G, Chen X. Imaging of integrins as biomarkers for tumor angiogenesis. Curr Pharm Des. 2008; 14:2943–73. [PubMed: 18991712]
8. Dijkgraaf I, Boerman OC. Radionuclide imaging of tumor angiogenesis. Cancer Biother Radiopharm. 2009; 24:637–47. [PubMed: 20025543]
9. Dallas NA, Samuel S, Xia L, Fan F, Gray MJ, Lim SJ, et al. Endoglin (CD105): a marker of tumor vasculature and potential target for therapy. Clin Cancer Res. 2008; 14:1931–7. [PubMed: 18381930]
10. Fonsatti E, Nicolay HJ, Altomonte M, Covre A, Maio M. Targeting cancer vasculature via endoglin/CD105: a novel antibody-based diagnostic and therapeutic strategy in solid tumours. Cardiovasc Res. 2010; 86:12–9. [PubMed: 19812043]
11. Seon BK, Haba A, Matsuno F, Takahashi N, Tsujie M, She X, et al. Endoglin-targeted cancer therapy. Curr Drug Deliv. 2011; 8:135–43. [PubMed: 21034418]
12. Cai W, Rao J, Gambhir SS, Chen X. How molecular imaging is speeding up antiangiogenic drug development. Mol Cancer Ther. 2006; 5:2624–33. [PubMed: 17121909]
13. Zhang Y, Yang Y, Hong H, Cai W. Multimodality molecular imaging of CD105 (Endoglin) expression. Int J Clin Exp Med. 2011; 4:32–42. [PubMed: 21394284]
14. Zhang D, Feng XY, Henning TD, Wen L, Lu WY, Pan H, et al. MR imaging of tumor angiogenesis using sterically stabilized Gd-DTPA liposomes targeted to CD105. Eur J Radiol. 2009; 70:180–9. [PubMed: 18541399]
15. Bredow S, Lewin M, Hofmann B, Marecos E, Weissleder R. Imaging of tumour neovasculature by targeting the TGF-beta binding receptor endoglin. Eur J Cancer. 2000; 36:675–81. [PubMed: 10738134]
16. Costello B, Li C, Duff S, Butterworth D, Khan A, Perkins M, et al. Perfusion of ^{99m}Tc-labeled CD105 Mab into kidneys from patients with renal carcinoma suggests that CD105 is a promising vascular target. Int J Cancer. 2004; 109:436–41. [PubMed: 14961584]
17. Fonsatti E, Jekunen AP, Kairemo KJ, Coral S, Snellman M, Nicotra MR, et al. Endoglin is a suitable target for efficient imaging of solid tumors: in vivo evidence in a canine mammary carcinoma model. Clin Cancer Res. 2000; 6:2037–43. [PubMed: 10815930]

18. Korpanty G, Carbon JG, Grayburn PA, Fleming JB, Brekken RA. Monitoring response to anticancer therapy by targeting microbubbles to tumor vasculature. Clin Cancer Res. 2007; 13:323–30. [PubMed: 17200371]
19. Korpanty G, Grayburn PA, Shohet RV, Brekken RA. Targeting vascular endothelium with avidin microbubbles. Ultrasound Med Biol. 2005; 31:1279–83. [PubMed: 16176794]
20. Cui S, Lu SZ, Chen YD, He GX, Liu JP, Song ZY, et al. Relationship between intravascular ultrasound imaging features of coronary plaques and soluble CD105 level in patients with coronary heart disease. Chin Med J (Engl). 2007; 120:595–7. [PubMed: 17442209]
21. Hong H, Yang Y, Zhang Y, Engle JW, Barnhart TE, Nickles RJ, et al. Positron emission tomography imaging of CD105 expression during tumor angiogenesis. Eur J Nucl Med Mol Imaging. 2011; 38:1335–43. [PubMed: 21373764]
22. Yang Y, Zhang Y, Hong H, Liu G, Leigh B, Cai W. In vivo near-infrared fluorescence imaging of CD105 expression during tumor angiogenesis. Eur J Nucl Med Mol Imaging. 2011 in press.
23. Lee SY, Hong YD, Felipe PM, Pyun MS, Choi SJ. Radiolabeling of monoclonal anti-CD105 with ^{177}Lu for potential use in radioimmunotherapy. Appl Radiat Isot. 2009; 67:1366–9. [PubMed: 19324561]
24. Mendelson DS, Gordon MS, Rosen LS, Hurwitz H, Wong MK, Adams BJ, et al. Phase I study of TRC105 (anti-CD105 [endoglin] antibody) therapy in patients with advanced refractory cancer. J Clin Oncol. 2010; 28:15s.
25. Meijs WE, Herscheid JDM, Haisma HJ, Pinedo HM. Evaluation of desferal as a bifunctional chelating agent for labeling antibodies with Zr-89. Int J Radiat Appl Instrum, A, Appl Radiat Isot. 1992; 43:1443–7.
26. Vosjan MJ, Perk LR, Visser GW, Budde M, Jurek P, Kiefer GE, et al. Conjugation and radiolabeling of monoclonal antibodies with zirconium-89 for PET imaging using the bifunctional chelate p-isothiocyanatobenzyl-desferrioxamine. Nat Protoc. 2010; 5:739–43. [PubMed: 20360768]
27. Perk LR, Vosjan MJ, Visser GW, Budde M, Jurek P, Kiefer GE, et al. p-Isothiocyanatobenzyl-desferrioxamine: a new bifunctional chelate for facile radiolabeling of monoclonal antibodies with zirconium-89 for immuno-PET imaging. Eur J Nucl Med Mol Imaging. 2010; 37:250–9. [PubMed: 19763566]
28. Wang H, Cai W, Chen K, Li ZB, Kashefi A, He L, et al. A new PET tracer specific for vascular endothelial growth factor receptor 2. Eur J Nucl Med Mol Imaging. 2007; 34:2001–10. [PubMed: 17694307]
29. Holland JP, Sheh Y, Lewis JS. Standardized methods for the production of high specific-activity zirconium-89. Nucl Med Biol. 2009; 36:729–39. [PubMed: 19720285]
30. Takahashi N, Haba A, Matsuno F, Seon BK. Antiangiogenic therapy of established tumors in human skin/severe combined immunodeficiency mouse chimeras by anti-endoglin (CD105) monoclonal antibodies, and synergy between anti-endoglin antibody and cyclophosphamide. Cancer Res. 2001; 61:7846–54. [PubMed: 11691802]
31. Cai W, Wu Y, Chen K, Cao Q, Tice DA, Chen X. *In vitro* and *in vivo* characterization of ^{64}Cu-labeled Abegrin^{TM}, a humanized monoclonal antibody against integrin $\alpha_v\beta_3$. Cancer Res. 2006; 66:9673–81. [PubMed: 17018625]
32. Cai W, Chen K, Mohamedali KA, Cao Q, Gambhir SS, Rosenblum MG, et al. PET of vascular endothelial growth factor receptor expression. J Nucl Med. 2006; 47:2048–56. [PubMed: 17138749]
33. Holland JP, Divilov V, Bander NH, Smith-Jones PM, Larson SM, Lewis JS. ^{89}Zr-DFO-J591 for immunoPET of prostate-specific membrane antigen expression in vivo. J Nucl Med. 2010; 51:1293–300. [PubMed: 20660376]
34. Borjesson PK, Jauw YW, Boellaard R, de Bree R, Comans EF, Roos JC, et al. Performance of immuno-positron emission tomography with zirconium-89-labeled chimeric monoclonal antibody U36 in the detection of lymph node metastases in head and neck cancer patients. Clin Cancer Res. 2006; 12:2133–40. [PubMed: 16609026]
35. Tsujie M, Uneda S, Tsai H, Seon BK. Effective anti-angiogenic therapy of established tumors in mice by naked anti-human endoglin (CD105) antibody: differences in growth rate and therapeutic

response between tumors growing at different sites. Int J Oncol. 2006; 29:1087–94. [PubMed: 17016638]

36. Matsuno F, Haruta Y, Kondo M, Tsai H, Barcos M, Seon BK. Induction of lasting complete regression of preformed distinct solid tumors by targeting the tumor vasculature using two new anti-endoglin monoclonal antibodies. Clin Cancer Res. 1999; 5:371–82. [PubMed: 10037187]
37. Cai W, Ebrahimnejad A, Chen K, Cao Q, Li ZB, Tice DA, et al. Quantitative radioimmunoPET imaging of EphA2 in tumor-bearing mice. Eur J Nucl Med Mol Imaging. 2007; 34:2024–36. [PubMed: 17673999]
38. Cai W, Chen K, He L, Cao Q, Koong A, Chen X. Quantitative PET of EGFR expression in xenograft-bearing mice using ^{64}Cu-labeled cetuximab, a chimeric anti-EGFR monoclonal antibody. Eur J Nucl Med Mol Imaging. 2007; 34:850–8. [PubMed: 17262214]
39. Heskamp S, van Laarhoven HW, Molkenboer-Kuenen JD, Franssen GM, Versleijen-Jonkers YM, Oyen WJ, et al. ImmunoSPECT and immunoPET of IGF-1R expression with the radiolabeled antibody R1507 in a triple-negative breast cancer model. J Nucl Med. 2010; 51:1565–72. [PubMed: 20847162]
40. Roopenian DC, Akilesh S. FcRn: the neonatal Fc receptor comes of age. Nat Rev Immunol. 2007; 7:715–25. [PubMed: 17703228]
41. Jefferis R, Lefranc MP. Human immunoglobulin allotypes: possible implications for immunogenicity. MAbs. 2009; 1:332–8. [PubMed: 20073133]

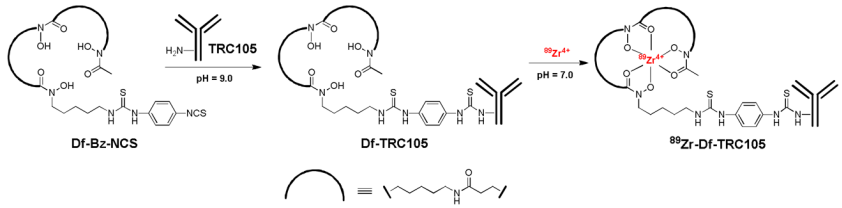

Fig. 1.
The 2-step procedure for ^{89}Zr-labeling of TRC105.

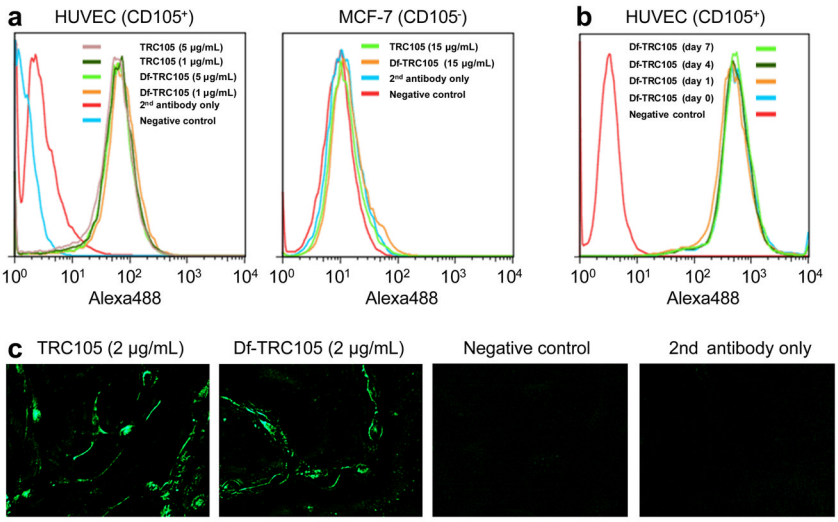

Fig. 2.

In vitro investigation of Df-TRC105. **a** Flow cytometry analysis of TRC105 and Df-TRC105 in HUVECs (CD105-positive) and MCF-7 (CD105-negative) cells at different concentrations. **b** Flow cytometry analysis of Df-TRC105 (4 μg/mL) in HUVECs after incubation in complete mouse serum at 37 °C for 1, 4, and 7 days. **c** Fluorescence microscopy images of HUVECs using either TRC105 or Df-TRC105 (2 μg/mL) as the primary antibody. Various control images are also shown.

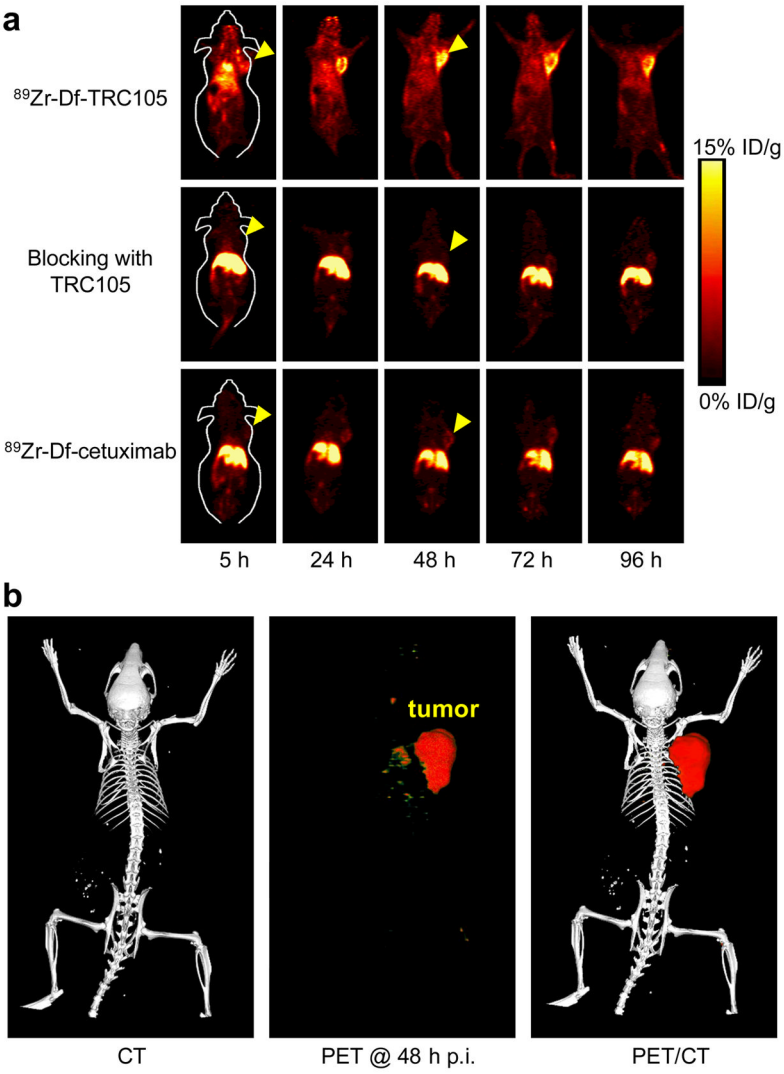

Fig. 3.

Small animal PET imaging of 4T1 tumor-bearing mice. **a** Serial coronal PET images at 5, 24, 48, 72, and 96 h post-injection of ^{89}Zr-Df-TRC105, 2 mg of TRC105 before ^{89}Zr-Df-TRC105 (i.e. blocking), or ^{89}Zr-Df-cetuximab. Tumors are indicated by arrowheads. **b** Representative PET/CT images of ^{89}Zr-Df-TRC105 in 4T1 tumor-bearing mice at 48 h post-injection.

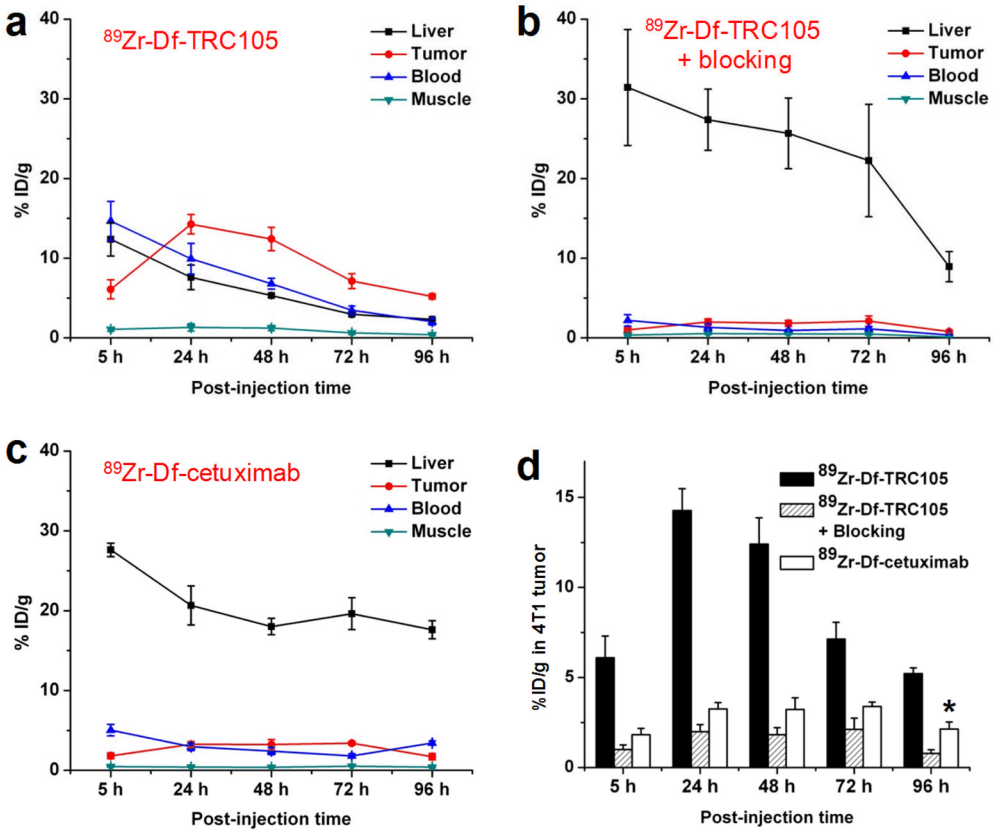

Fig. 4.

Quantitative ROI analysis of the PET data. **a** Time-activity curves of the tumor, liver, blood, and muscle upon intravenous injection of ^{89}Zr-Df-TRC105 into 4T1 tumor-bearing mice (n = 4). **b** Time-activity curves of the tumor, liver, blood, and muscle upon intravenous injection of ^{89}Zr-Df-TRC105, after a blocking dose of TRC105, into 4T1 tumor-bearing mice (n = 4). **c** Time-activity curves of the tumor, liver, blood, and muscle upon intravenous injection of ^{89}Zr-Df-cetuximab into 4T1 tumor-bearing mice (n = 4). **d** Comparison of the 4T1 tumor uptake of ^{89}Zr-Df-TRC105, ^{89}Zr-Df-TRC105 after a blocking dose of TRC105, and ^{89}Zr-Df-cetuximab. P values are < 0.01 in all cases when compared with ^{89}Zr-Df-TRC105, except one case where P < 0.05 (denoted with “*”).

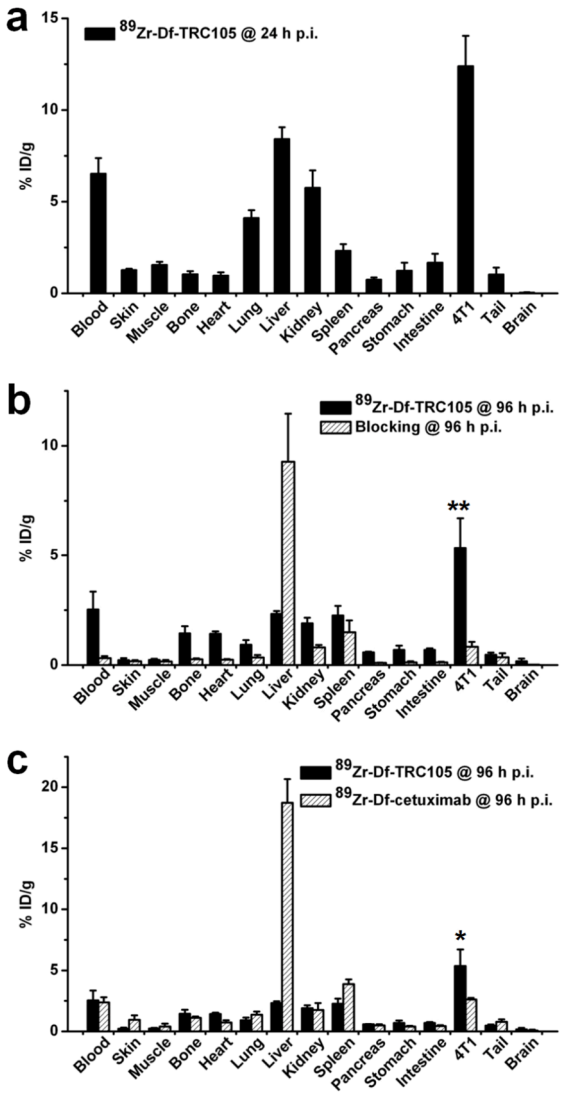

Fig. 5.

Biodistribution studies in 4T1 tumor-bearing mice. **a** Biodistribution of ^{89}Zr-Df-TRC105 at 24 h post-injection (n = 4). **b** Biodistribution of ^{89}Zr-Df-TRC105 and ^{89}Zr-Df-TRC105 after a blocking dose of TRC105 at 96 h post-injection (n = 4). **c** Biodistribution of ^{89}Zr-Df-TRC105 and ^{89}Zr-Df-cetuximab at 96 h post-injection (n = 4). *: $P < 0.05$; **: $P < 0.01$.

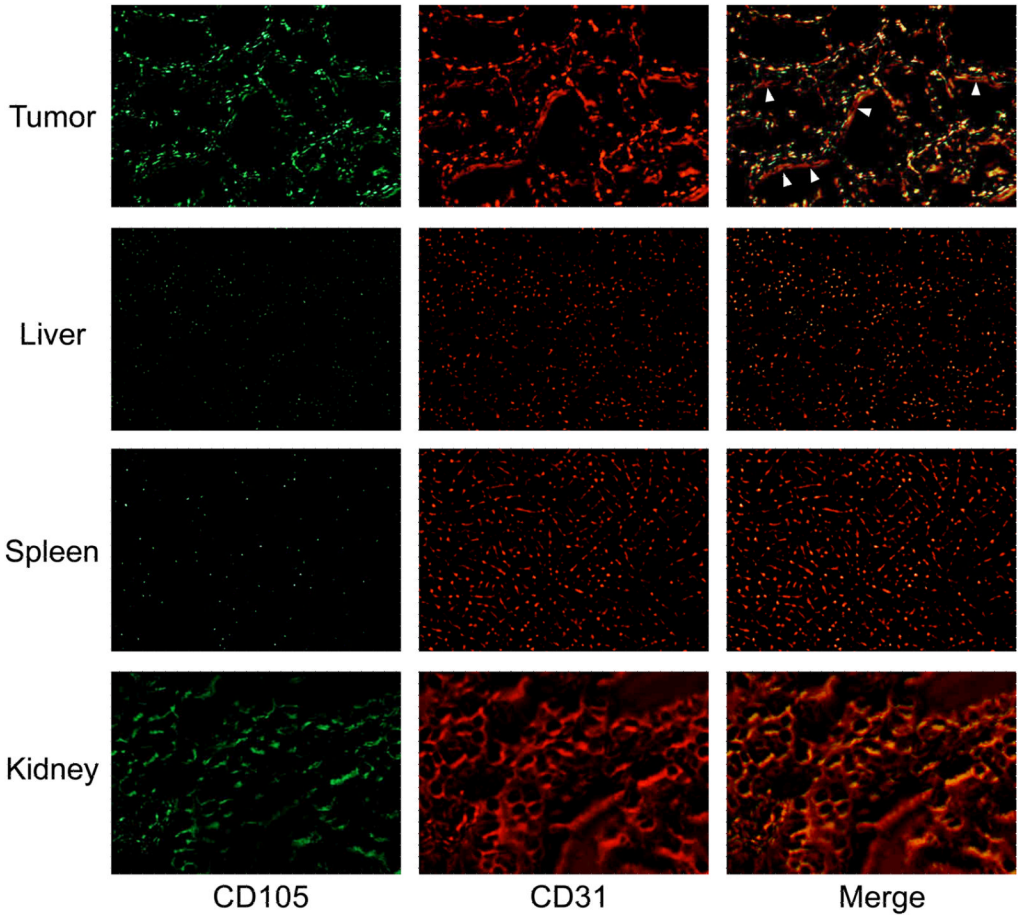

Fig. 6.

Immunofluorescence CD105/CD31 double-staining of the 4T1 tumor, liver, spleen, and kidney tissue sections. TRC105 and AlexaFluor488-labeled goat anti-human IgG were used for CD105 staining (green). Afterwards, the tissue slices were stained with rat anti-mouse CD31 antibody and Cy3-labeled donkey anti-rat IgG (red). Note that CD105 expression was high on newly formed blood vessels but not on mature vessels, which exhibited predominantly CD31 staining (indicated by arrowheads). CD105 expression levels in the liver and spleen are much lower than in the tumor vessels. Significant level of CD105 expression was also observed in the renal medulla. All images were acquired under the same condition and displayed at the same scale. Magnification: 200×.